

# 3D Covalent Organic Frameworks with 16-Connectivity for Photocatalytic C(sp<sup>3</sup>)–C(sp<sup>2</sup>) Cross-Coupling

Meng Lu, Shuai-Bing Zhang, Run-Han Li, Long-Zhang Dong, Ming-Yi Yang, Pei Huang, Yu-Fei Liu, Ze-Hui Li, Han Zhang, Mi Zhang,\* Shun-Li Li, and Ya-Qian Lan\*



Cite This: <https://doi.org/10.1021/jacs.4c08951>



Read Online

ACCESS |



Metrics & More

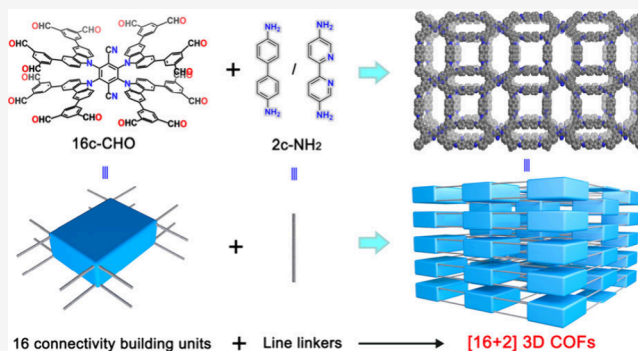


Article Recommendations



Supporting Information

**ABSTRACT:** The connectivity (valency) of building blocks for constructing 3D covalent organic frameworks (COFs) has long been limited to 4, 6, 8, and 12. Developing a higher connectivity remains a great challenge in the field of COF structural design. Herein, this work reports a hierarchical expansion strategy for making 16-connected building blocks to construct 3D COFs with sqc topology. The [16 + 2] construction achieved by condensation between a 16-connected carbazoyl dicyanobenzene-based building block (CzTPN) and linear diamino linkers (BD or Bpy) affords two 3D COFs (named CzBD COF and CzBpy COF). Furthermore, attributed to the well-organized donor–acceptor (D–A) heterojunction, the Ni chelated CzBpy COF (Ni@CzBpy COF) exhibits excellent performance for photoredox/Ni dual catalytic C(sp<sup>3</sup>)–C(sp<sup>2</sup>) cross-coupling of alkyltrifluoroborates with aryl halides, achieving a maximum 98% conversion and 94% yield for various substrates. This work developed the first case of high-connectivity COFs bearing 16-connected units, which is the highest connectivity reported until now, and achieved efficient photocatalysis applications, thus greatly enriching the possibilities of COFs.



## INTRODUCTION

Covalent organic frameworks (COFs), as an emerging class of well-defined crystalline materials with flexible structural designability and functionality, have attracted enormous attention.<sup>1–9</sup> In this field, the design of two-dimensional (2D) COFs has been well developed, and various building units have been reported.<sup>10–13</sup> However, the development of three-dimensional (3D) COFs has been relatively limited due to the lower availability of organic building blocks that form highly connected 3D geometries.<sup>14–19</sup> The discovery of new, readily accessible building blocks is the key to the design and discovery of new 3D COF platforms.

Up to now, the connectivity (valency) of single building blocks for COFs has generally been low ( $n \leq 12$ , building units with connectivity  $n$  are denoted as  $n$ -connected, abbreviated as  $n$ -c), and producing building units with higher connectivity is a well-known great challenge.<sup>18,20–23</sup> As is widely studied, the 4-connected tetrahedral (Td) net is the most commonly explored three-periodic COF platform.<sup>24–30</sup> Furthermore, 6-c and 8-c building units have also been developed for designing 3D COFs.<sup>17,31–36</sup> An early example of a high-connected COF was reported by Yaghi et al., making COFs with 8-c or infinite one-dimensional chain building blocks, which was great progress for designing high-valency COFs.<sup>15</sup> Recently, 12-connected 3D COFs were also reported.<sup>37</sup> However,

constructing higher-connectivity ( $n > 12$ ) building units with 3D geometries to further boost the structural development of 3D COFs has rarely been achieved. Especially, the COF design based on 16-c building units has not been reported. In this study, to break through the limitation of connectivity, we rationally designed a 16-c building unit suitable for the practice of reticular chemistry to construct the highest-connected 3D COFs.

Herein, a 16-c building block, termed 2,3,5,6-tetrakis(3,6-bis(3,5-diformylphenyl)-9H-carbazol-9-yl)terephthalonitrile (named CzTPN-16CHO) was synthesized and then condensed with two linear diamino linkers (4,4'-biphenylenediamine (BD) and 2,2'-bipyridine-5,5'-diamine (Bpy)) by a Schiff base reaction, which produced two high crystalline 3D COFs (named CzBD COF and CzBpy COF) with sqc topology (Figure 1). Benefiting from the high surface area, periodic skeleton, and abundant exposed Ni coordinated moieties in the frameworks, the Ni chelated CzBpy COF (Ni@

**Received:** July 2, 2024

**Revised:** August 26, 2024

**Accepted:** August 27, 2024

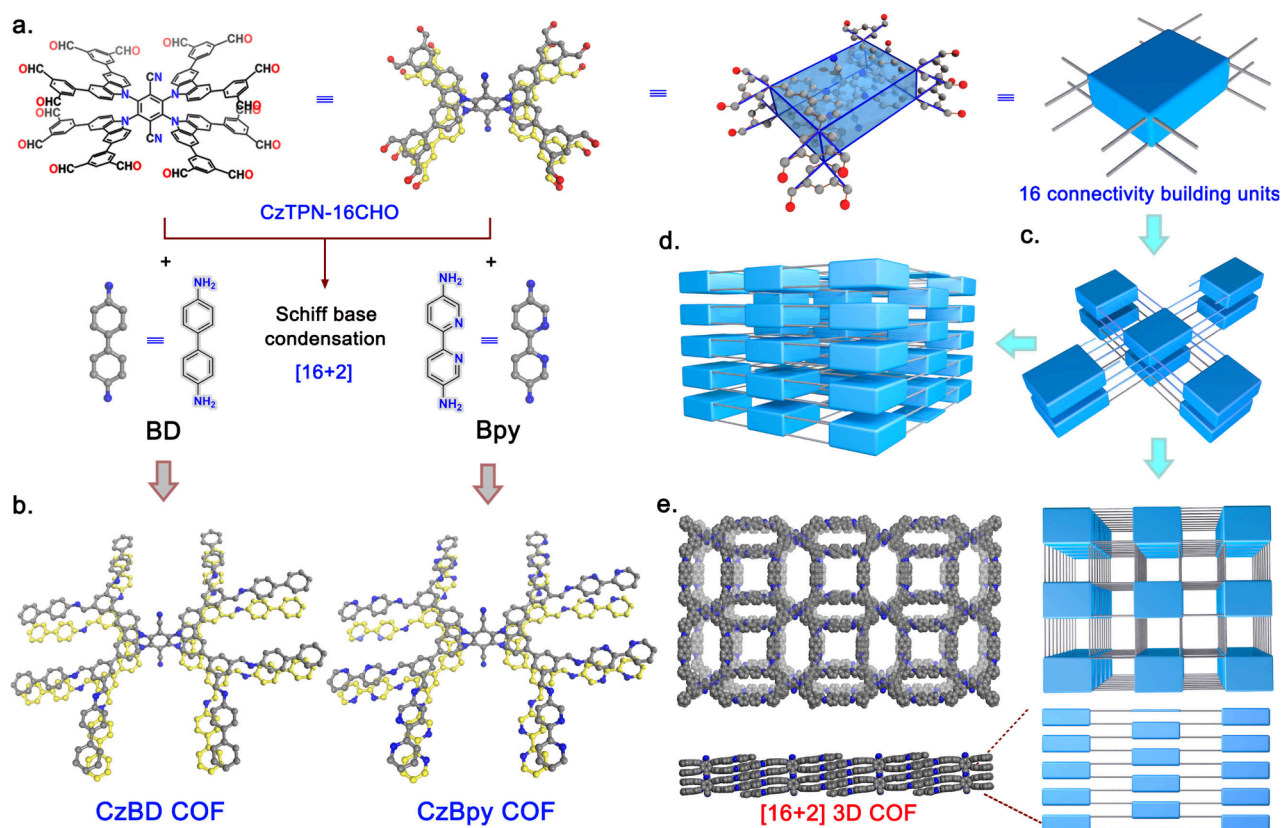


**Figure 1.** Synthesis and structure of 16-c building unit-based [16 + 2] 3D COFs. (a) Molecular structure of CzTPN-16CHO as a 16-c building block evolving into a geometric structure with 16 unsaturated sites. (b) Structure segments of two [16 + 2] COFs, CzBD COF and CzBpy COF. (c, d) Schematic diagram of assembly mode. (e) Crystal structure for CzBD COF and its topological representation from top and side views.

CzBpy COF) crystalline materials were successfully used as photocatalysts for photoredox/Ni dual catalytic C(sp<sup>3</sup>)–C(sp<sup>2</sup>) cross-coupling of alkyltrifluoroborates with aryl halides under visible light irradiation and achieved high conversions (98%) for many examples. In addition, a possible reaction mechanism was proposed with the assistance of DFT calculations. The theoretical calculations also delineated the feasibility of electron transfer from the photosensitive CzTPN center to the catalytically active Ni center inside these COFs, as well as the photocatalytic cycle and Ni-catalytic cycle on CzTPN and Ni-dipyridyl, respectively. Above all, this study is the first introduction to the construction of COFs derived from the (16, 2)-c net as a means to access the 16-c building unit, which is a breakthrough in connectivity in the field of 3D COFs and expands the library of building blocks for the development of COF structures.

## RESULTS AND DISCUSSION

**Design and Synthesis of 16-c-Based COFs.** We proposed a hierarchical expansion strategy to access 16-c building units (Figure 2). By stepwise expansion of the functional groups, rationally designed building units with specific connectivity can be obtained. After receiving 16-c units, two target [16 + 2] COFs (CzBD COF and CzBpy COF) were synthesized by condensation of CzTPN-16CHO with BD/Bpy under solvothermal conditions with aniline as a modulator (Figures S1 and S2).<sup>25</sup>

The crystal structure of the two COFs was first characterized by powder X-ray diffraction (PXRD) combined with theoretical structural simulations. The PXRD analysis con-

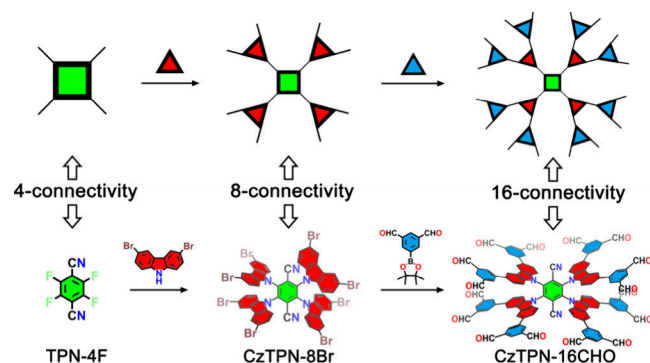


**Figure 2.** Hierarchical expansion strategy to access 16-c building units and the construction path of CzTPN-16CHO.

firmed the crystallinity of the two COFs and revealed no diffraction peaks that could be attributed to residual starting materials (Figures S3 and S4). In these reticular frameworks (Figure 1a,b), the CzTPN units with 16 aldehyde groups act as the 16-connected nodes and the linker ligands BD and Bpy act as the 2-connected building blocks, forming an edge transitive (16, 2)-connected net (Figure 1c–e).

Structural analysis via PXRD revealed that both COFs exhibited prominent peaks at 3.67°, 6.12°, 7.20°, and 10.05°, which were assigned to the 100, 200, 150, and 160 reflections in the raw simulated structural mode, respectively. The experimental PXRD diffractions matched well with the calculated results based on an sqc topology structure, simplified to an (8, 3) network structure. In addition, the

Rietveld refinement for CzBD COF and CzBpy COF fit well with the experimental results, with convergence to  $R_p = 4.33\%$ / $R_{wp} = 5.66\%$  and  $R_p = 5.43\%$ / $R_{wp} = 7.36\%$ , respectively, suggesting the validity of the computational model (Figure 3a,b). 2D stacking models of CzBD COF and Bpy COF with

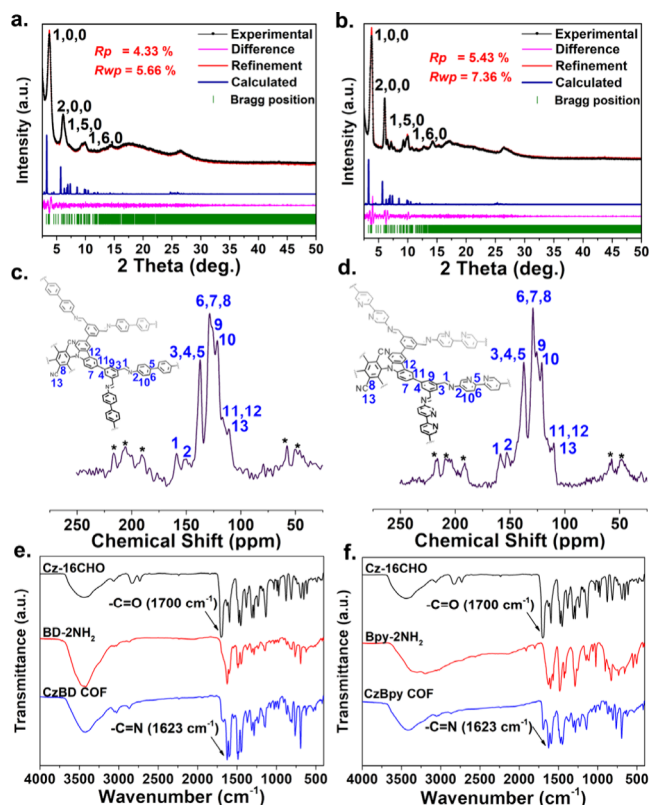


**Figure 3.** Structure characterizations. Experimental and simulated PXRD patterns of (a) CzBD COF and (b) CzBpy COF. ssNMR spectra of (c) CzBD COF and (d) CzBpy COF. Asterisks denote satellite or peak spinning side band signals. FT-IR spectra of (e) CzBD COF and (f) CzBpy COF.

sql topology were also simulated, but the calculated PXRD had discrepancies with the experiments, which ruled out the possibility of such structures (Figure S45–S50).  $^{13}\text{C}$  solid-state NMR (ssNMR) spectroscopy was then performed to validate the formation and connectivity of the building units (Figure 3c,d). The characteristic peak at ca. 159 ppm in the  $^{13}\text{C}$  ssNMR spectra corresponded to the carbon atom of the C=N bond.<sup>5,38</sup> In addition, the appearance of a new peak at  $1623\text{ cm}^{-1}$  in the Fourier transform infrared (FT-IR) spectra can be assigned to the telescopic vibration of an imine bond (—C=N) (Figure 3e,f).<sup>39,40</sup> The above results confirmed the successful Schiff base condensation reaction required for these COFs.

The morphology of CzBD COF and CzBpy COF was characterized by scanning electron microscopy (SEM) and transmission electron microscopy (TEM), which indicated a single morphological phase with a distribution of crystal sizes of  $\sim 2$  to  $10\text{ }\mu\text{m}$  for CzBpy COF and  $\sim 1$  to  $3\text{ }\mu\text{m}$  for CzBD COF (Figure 4a and Figure S6). Their highly regular structures were also investigated by high-resolution TEM (HRTEM). As shown in Figure 4b and Figure S7, the spacing of the lattice fringe ( $\sim 3.6\text{ }\text{\AA}$ ) corresponded to the lattice planes of (001) in the CzBpy COF, which indicated the distance between

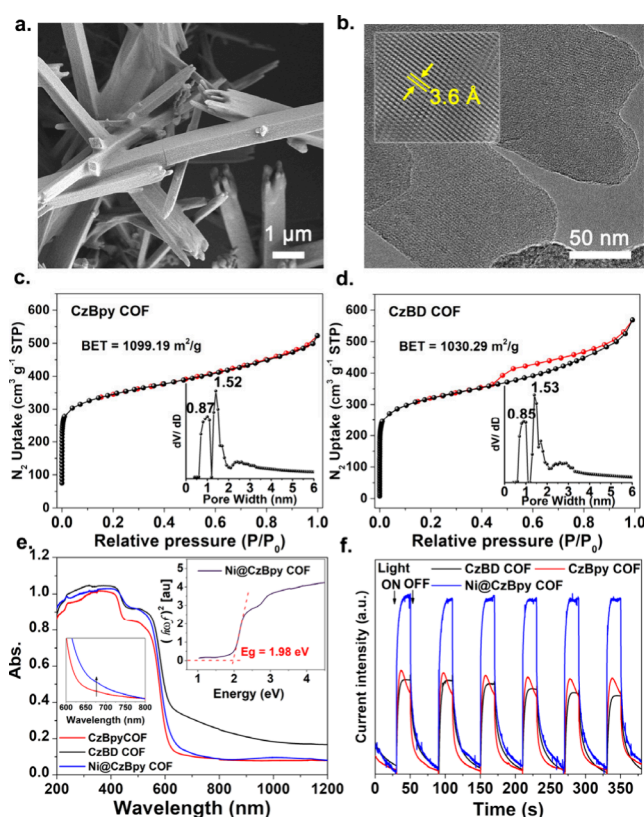


**Figure 4.** (a) SEM and (b) HRTEM images of CzBpy COF.  $\text{N}_2$  adsorption isotherm and pore size distribution of (c) CzBpy COF and (d) CzBD COF. (e) UV-vis absorption spectra and (f) transient photocurrent response of CzBD COF, CzBpy COF, and Ni@CzBpy COF.

adjacent layers of the CzTPN fragment. To evaluate the surface area and porosity of CzBD COF and CzBpy COF,  $\text{N}_2$  adsorption isotherms were collected at  $77\text{ K}$ . As shown in Figure 4c,d, the sharp increase in the low-pressure range ( $P/P_0 < 0.05$ ) indicated the typical type I isotherm for both COFs. Accordingly, the Brunauer–Emmett–Teller (BET) specific surface areas were calculated to be  $1099.2\text{ m}^2/\text{g}$  for CzBpy COF and  $1030.3\text{ m}^2/\text{g}$  for CzBD COF. The pore distribution was also calculated for both COFs by using the nonlocal density functional theory (NLDFT) model. Both CzBpy COF and CzBD COF possessed two major micro-sized pores with pore sizes of  $\sim 0.9$  and  $\sim 1.5\text{ nm}$ , which is consistent with the simulated crystal structure. We then performed an elemental analysis (EA) test for the COFs, and the results are shown as Table S1. As expected, the test results were in line with the theoretical contents, which further support the purity of the obtained COF products.

The thermal and chemical stability of these COFs were studied by thermogravimetric analysis (TGA) and solvent immersion experiments. CzBD/Bpy COFs were observed to be chemically stable in various organic solvents, including *N,N*-dimethylformamide (DMF), dimethylsulfoxide (DMSO), methanol (MeOH), acetonitrile (ACN), and tetrahydrofuran (THF). After being immersed in these solvents for 3 days, CzBD/Bpy COFs retained their crystallinity (Figures S23 and S24). It is noted that the PXRD peak intensity became weaker in some solvents; however, the peak position was still maintained. The reason for the weakening of PXRD peaks can be attributed to the residual solvent interacting with the



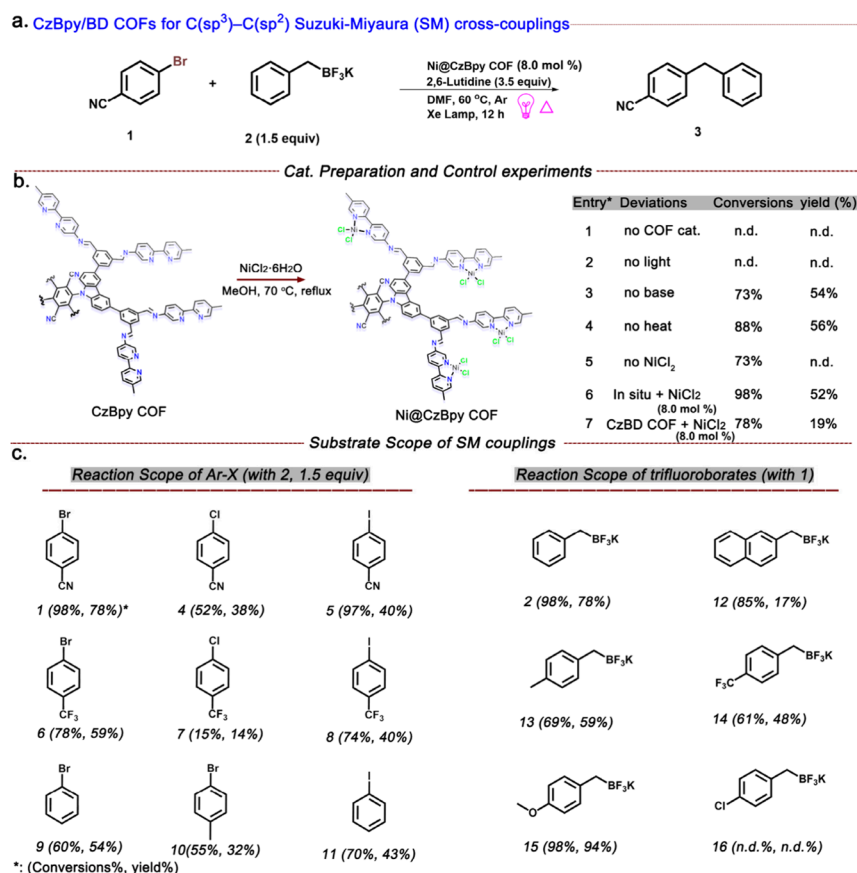


**Figure 5.** (a) SM cross-couplings of trifluoroborates and aryl bromides with Ni@CzBpy COF. (b) Synthesis of Ni@CzBpy COF and control experiments for SM cross-coupling reactions. (c) The substrate scope of SM couplings. Typical test conditions: aryl halides (0.05 mmol), alkyltrifluoroborates (0.075 mmol, 1.5 equiv), COF catalyst (2 mg, 8.0 mol % Ni catalyst), DMF (1 mL), and 2,6-lutidine (0.04 mL).

related crystal plane. To prove the above hypothesis, we then tried to remove solvents by washing and treating the COFs with Soxhlet extractions with THF and studied their influence on the PXRD patterns. Interestingly, the PXRD intensity of the above resulting COFs was obviously enhanced. However, these COFs were unstable in acid solutions. In particular, CzBD/Bpy COFs quickly decomposed in 1 M HCl. The TGA results revealed that CzBD/Bpy COFs did not decompose until 300 °C under nitrogen and could be stable under an oxygen atmosphere until 360 °C (Figures S17–S22).

**Photophysical and Photocatalytic Properties of COFs.** The carbazole-based fluorophore is widely considered to be a potential photocatalyst for photoredox reactions.<sup>41–43</sup> Nickel has the ability to mediate free radical cross-coupling reactions and has been extensively studied in metal photoredox catalysis and energy transfer catalysis.<sup>44–49</sup> Herein, the coupling of photosensitizing CzTPN and nickel centers within the COF will be a good way to create a dual photoredox Ni@CzBpy COF catalyst for the visible-light-mediated C(sp<sup>3</sup>)-C(sp<sup>2</sup>) Suzuki–Miyaura (SM) cross-coupling of alkyltrifluoroborates with aryl halides.<sup>50</sup> In this system, the energy or electron transfer between the CzTPN and a thermodynamically stable Ni(II) intermediate triggers reductive elimination of the desired product.<sup>51</sup>

Based on the above discussions, we then designed a photosensitizer-Ni catalytic center coupled photoredox catalyst by coordinating Ni(II) centers to these CzTPN-based COFs through bipyridine moieties.<sup>52</sup> CzBpy COF was metalated with NiCl<sub>2</sub>·6H<sub>2</sub>O in a MeOH mixture at 70 °C for 24 h to afford

Ni@CzBpy COF. The PXRD pattern showed the complex remained highly crystalline compared to raw CzBpy COF (Figure S5). The FT-IR spectrum showed that the  $\nu(\text{C}=\text{N})$  stretching vibration band at 1623 cm<sup>-1</sup> still existed (Figure S11), and the <sup>13</sup>C CP/MAS solid-state NMR spectrum of Ni@CzBpy COF showed that the peak at 159 ppm was attributed to the C of the imine bond (Figure S16). All of these results showed the preservation of the chemical structure. The X-ray photoelectron spectroscopy (XPS) results indicated the presence of Ni in Ni@CzBpy COF (Figures S12 and S13). The Ni 2p<sub>1/2</sub> and Ni 2p<sub>3/2</sub> binding energies of 873.3 and 855.7 eV in Ni@CzBpy COF, respectively, suggested the divalent nature of Ni centers.<sup>50</sup>

The FT-IR integrated with fine N 1s XPS (Figure S14) analysis indicated that Ni was coordinated with N and Cl atoms. The DFT method was then conducted to study the coordination structure configuration of Ni in Ni@CzBpy COF. As a result, combined with the experimental and theoretical coordination geometry of Ni(II), we concluded that the possible coordination mode of Ni in Ni@CzBpy COF was [NiCl<sub>2</sub>(bipyridine)] (Figure S15), which formed four-coordinated Ni(II) complexes with the Ni atom being coordinated by two N atoms of the bipyridine ligand and two chlorides.<sup>53,54</sup> Inductively coupled plasma optical emission spectrometry (ICP-OES) analysis indicated there was 12.7 wt % nickel in the Ni@CzBpy COF. The SEM and TEM results showed that Ni@CzBpy COF retained its morphology with CzBpy COF (Figures S8 and S9). The EDX elemental mapping of Ni@CzBpy COF signified that C, N, and Ni were evenly

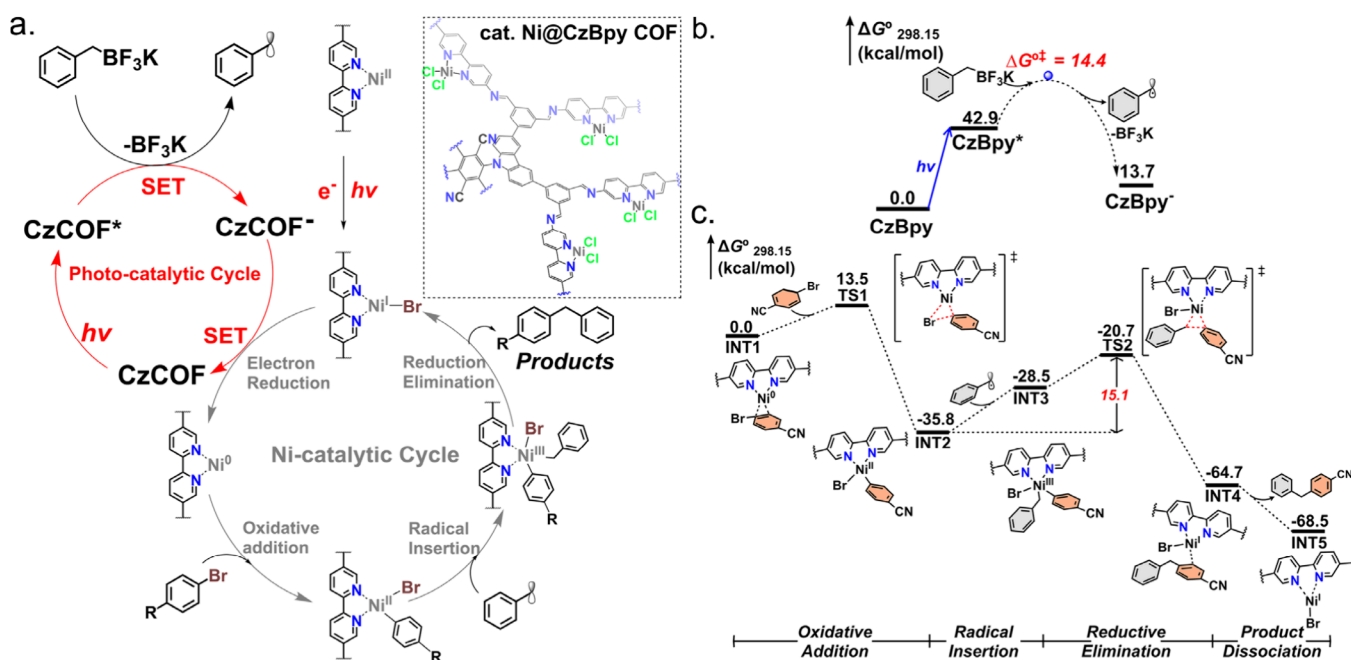


**Figure 6.** (a) Proposed mechanism of Ni@CzBpy COF for photoredox/Ni dual catalytic C(sp<sup>3</sup>)–C(sp<sup>2</sup>) cross-coupling. (b) Calculated free energy profiles for degradation of aryl-BF<sub>3</sub>K nucleophiles to generate an aryl radical over CzBpy sites. (c) Calculated free energy profiles for Ni-catalytic cycle for C(sp<sup>3</sup>)–C(sp<sup>2</sup>) cross-coupling, including oxidative addition, radical insertion, reductive elimination, and product dissociation processes. The values are given in units of kcal/mol.

distributed within the structure (Figure S10), which demonstrated the homogeneous distribution of Ni in COF substrates.

Solid-state UV–vis absorption spectra and transient photocurrent responses were then obtained to evaluate the optoelectronic properties of the obtained COFs. The UV–vis absorption results showed that both CzBpy COF and CzBD COF exhibit broad light absorption over all of the visible light range (Figure 4e and Figures S29–S32). Especially, Ni@CzBpy COF exhibited a stronger light absorption intensity than CzBpy COF, which was related to the increased degree of electron delocalization due to the chelation of Ni. The incorporation of Ni decreased the bandgap ( $E_g$ ) to 1.98 eV in the Ni@CzBpy COF (Figure 4e, inset), suggesting that it is a good candidate for photocatalysts.<sup>55,56</sup> The Tauc plot from the UV–vis absorption spectra coupled with the Mott–Schottky plots confirmed the band structures of these photocatalysts (Figures S33–S36).

The intensity of the transient photocurrent response showed that Ni@CzBpy COF had the highest intensity compared to other COFs (Figure 4f), which suggested superior photo-induced electron separation and transport efficiency. The band structure was then studied with the assistance of the Mott–Schottky test, which showed that Ni@CzBpy COF possessed stronger reduction potential. These results revealed that Ni@CzBpy COF possessed good light harvesting ability, charge separation, and transport properties, which suggested that Ni@CzBpy COF may be a good candidate for visible-light-mediated nickel catalyzed cross-coupling reactions.

The photocatalytic performance of Ni@CzBpy COF was first studied in C(sp<sup>3</sup>)–C(sp<sup>2</sup>) SM cross-couplings between alkyltrifluoroborates (R-BF<sub>3</sub>K) and aryl halides (Figure 5a). Upon irradiation with a Xe lamp at 60 °C, a DMF solution of 4-bromobenzonitrile (1) and potassium benzyl trifluoroborate (2) in the presence of Ni@CzBpy COF (8.0 mol % Ni

catalyst) and 2,6-lutidine (3.5 equiv as base) was stirred at room temperature for 12 h, affording 4-benzylbenzonitrile (3) in 78% yield. We then conducted control experiments to study the reaction conditions (Figure 5b). The results revealed that no product was formed in the absence of a COF catalyst (entry 1) or light irradiation (entry 2). Besides, the removal of the base (2,6-lutidine) only gave a minor conversion to 3 (entry 3). The conversions and yields largely decreased after the removal of heat by conducting a photoreaction at room temperature and only obtained yields of 56% (entry 4). Interestingly, the removal of NiCl<sub>2</sub> gave mostly degradation of 4-bromobenzonitrile to benzonitrile, while no product 3 was observed (entry 5). The dehalogenation of aryl halides resulted from the photoinduced reductive elimination of 4-bromobenzonitrile by CzTPN of the COFs, which we discuss in the following. Furthermore, the CzBD COF was also studied as a photoredox catalyst for SM cross-couplings. In the case of the addition of NiCl<sub>2</sub> to the reaction system, the product yield reached 19%, which is much lower than that obtained with Ni@CzBpy COF. The results also confirmed that dipyrindyl nickel plays an important role in catalytic reactions. Above all, the control experiments indicated that Ni@COFs, light, ligand, base, and heat were all indispensable to realize this transformation efficiently. The substrate scope of SM couplings (Figure 5c) showed that various aryl halides including bromides, iodides, chlorides, and various alkyltrifluoroborates including electron-withdrawing/donating groups were all tolerated under this catalytic system, achieving a maximum conversion of 98% with 94% yield, which showed one of the best performances among previously reported photoredox/Ni dual catalytic C(sp<sup>3</sup>)–C(sp<sup>2</sup>) cross-coupling reaction catalysts (Table S2). The structural integrity of Ni@CzBpy COF was retained after the reaction, as confirmed by PXRD, FT-IR, XPS, and TEM characterizations (Figures S25–S28).

### Studies on the Photocatalytic Reaction Mechanism.

Having determined the optimal conditions for the cross-couplings between alkyltrifluoroborates and aryl halides over the COF catalyst, we investigated the general applicability of the transformation. We first explored the reaction scope of aryl halides with potassium benzyl trifluoroborate by Ni@CzBpy COF. The performance of aryl halides bearing different substitution patterns was evaluated, including bromides, iodides, and chlorides, which were all successfully coupled with potassium benzyl trifluoroborate (Figures S37–S44). The aryl bromide (1, 6, 9) showed the highest activity of the coupling reaction, with 78% yield for 4-bromobenzonitrile and 59% yield for 4-bromobenzotrifluoride. Besides, the electron-withdrawing groups such as trifluoromethyl or nitrile and electron-donating groups such as methyl were also tolerated under our optimal conditions. 4-Bromotoluene (10) showed the weakest activity for the coupling reaction with only 32% yield. For the reaction scope of R-BF<sub>3</sub>K, various alkyltrifluoroborates, including those substituted by phenyl (12), methyl (13), trifluoromethyl (14), methoxy (15), and chloro (16) groups were studied. Among them, the methoxy substituted alkyltrifluoroborates showed the highest performance with 94% yield, and the chloro-alkyltrifluoroborates showed no activity. It can be drawn that the effect of the electron-withdrawing/ donating group on the reaction yield is not a linear dependence. In this catalytic process with COFs as heterogeneous catalysts, the reaction efficiency will also be influenced by the complicated interactions between different substrates and the COF catalysts.

To study the mechanism of Ni@CzBpy COF as a photocatalyst for C(sp<sup>3</sup>)–C(sp<sup>2</sup>) cross-coupling reactions, time-dependent density functional theory (TDDFT) calculations were first used to compute the electronic structures of the Ni@CzBpy COF complex (Figure S51). As expected, for CzBpy COF (without Ni), the well-known electron acceptors dicyanoarene and carbazole fragment dominate the LUMO sites, while the HOMO site was mainly contributed by the dipyriddy part. However, after the partial chelation with NiCl<sub>2</sub>, the LUMO sites were mainly distributed at the Ni-dipyriddy part, suggesting that the photoinduced electron transfer (PET) process occurred from CzTPN to Ni-dipyriddy by light irradiation.

Based on the above results, we proposed that the photocatalytic cycle was originated by photoexciting CzBpy COF (abbreviated as CzCOF in Figure 6) to generate an excited-state CzCOF\*, driving two single electron transfer (SET) processes to initiate the catalytic reaction. Herein, a possible mechanism can be proposed: as shown in Figure 6a, the reaction is initiated by the photoreduction of Ni(II)@CzBpy COF to a Ni(I)@CzBpy COF catalyst, eliminating the coordinated chlorides. Then, this further goes through an electron reduction process to get a Ni(0) species. Next, oxidative addition to the C(sp<sup>2</sup>) precursor R-aryl halide substrate generates an R-aryl-Ni(II) complex. Meanwhile, CzCOF is excited by light irradiation to generate CzCOF\*. After that, an SET process occurs and generates an organic radical (Ar•) from the C(sp<sup>3</sup>) precursor (Ar-BF<sub>3</sub>K), which is subsequently captured by the R-aryl-Ni(II) complex through radical insertion, forming an R-aryl-Ni(III)-Ar species that readily undergoes reductive elimination. Finally, the C(sp<sup>2</sup>)–C(sp<sup>3</sup>) products R-aryl-Ar are dissociated from Ni-dipyriddy sites. Meanwhile, the Ni complex back in the Ni(I) @CzBpy COF state then participates in the next reaction cycle. To

study the initial process for Ni(I) as catalysts, we then conducted an in situ XPS test under the conditions of light irradiation in the presence of alkyl borate as a reductant. The results showed that the binding energy of Ni 2p<sub>3/2</sub> shifted to 854.6 eV under constant light irradiation (Figure S52), which was reduced by 1.1 eV compared to that of raw Ni@CzBpy COF (855.7 eV). Therefore, the obvious decrease in Ni 2p<sub>3/2</sub> binding energy proves that the valence of Ni gradually changes from Ni(II) to Ni(I) or a lower state.<sup>57</sup>

Figure 6b shows the calculated free energy profiles for the degradation of aryl-BF<sub>3</sub>K nucleophiles to generate aryl radicals over the CzBpy sites. In this process, the photoexcitation of CzBpy to CzBpy\* was the rate-determining step (RDS), which can be overcome by a strong light absorption ability and suitable bandgap. After that, the complex undergoes a facile oxidative reaction to generate Ar• from the Ar-BF<sub>3</sub>K by stripping –BF<sub>3</sub>K, with the overall barrier being only 14.4 kcal/mol in this step, simultaneously leading to a CzBpy<sup>–</sup> intermediate with a ~29.2 kcal/mol decrease in energy. In the Ni-catalytic cycle (Figure 6c), the free energy profiles of oxidative addition, radical insertion, reductive elimination, and product dissociation processes were all calculated. DFT calculations determined that the activation free energy for the oxidative addition of 4-bromobenzonitrile to INT1 via transition state TS1 was 13.5 kcal/mol, which is considered to be the rate-limiting step. Then, the Br<sup>–</sup> in radical TS1 can be dissociated to the aryl to INT2 in an event that was calculated to be exergonic by 49.3 kcal/mol. After that, the Ar• radical is inserted into the benzonitrile-Ni (II) complex via TS2, with an uphill free energy of 15.1 kcal/mol. At the last stage of the reaction, that is, the reductive elimination and product dissociation processes, all are exothermic spontaneous reactions. Finally, the C(sp<sup>3</sup>)–C(sp<sup>2</sup>) cross-coupling products are obtained.

## CONCLUSIONS

In summary, we have developed a hierarchical expansion strategy to design building blocks with 16-connectivity and successfully constructed two (16, 2)-connected COFs. This work breaks through the dilemma that the connectivity of building units for COFs is no more than 12 at the state of the art and first introduces a recorded connectivity with a 16-c building unit, thus expanding the library of building units for the design of COF structures. In addition, Ni@CzBpy COF can be used as photoredox catalyst for the C(sp<sup>3</sup>)–C(sp<sup>2</sup>) cross-coupling of alkyltrifluoroborates with aryl halides, achieving a maximum conversion of 98% with 94% yield. Various aryl halides including bromides, iodides, chlorides, and various alkyltrifluoroborates including electron-withdrawing/ donating groups were tolerated under this catalytic system. DFT calculations with a free energy profiles analysis were used to study the mechanism of Ni@CzBpy COF as a photocatalyst for this C(sp<sup>3</sup>)–C(sp<sup>2</sup>) cross-coupling reaction. We expect our hierarchical expansion strategy to be broadly applicable for designing higher-connected COFs and functional COFs for specific applications such as photocatalysis and electrocatalysis.

## ASSOCIATED CONTENT

### Supporting Information

The Supporting Information is available free of charge at <https://pubs.acs.org/doi/10.1021/jacs.4c08951>.



Experimental methods, characterization analyses and additional data, DFT calculations, and simulations for theoretical COF structures (PDF)

## AUTHOR INFORMATION

### Corresponding Authors

**Ya-Qian Lan** – Guangdong Provincial Key Laboratory of Carbon Dioxide Resource Utilization, School of Chemistry, South China Normal University, Guangzhou 510006, P.R. China; [orcid.org/0000-0002-2140-7980](https://orcid.org/0000-0002-2140-7980); Email: [yqlan@m.scnu.edu.cn](mailto:yqlan@m.scnu.edu.cn)

**Mi Zhang** – Guangdong Provincial Key Laboratory of Carbon Dioxide Resource Utilization, School of Chemistry, South China Normal University, Guangzhou 510006, P.R. China; Email: [mizhang@m.scnu.edu.cn](mailto:mizhang@m.scnu.edu.cn)

### Authors

**Meng Lu** – Guangdong Provincial Key Laboratory of Carbon Dioxide Resource Utilization, School of Chemistry, South China Normal University, Guangzhou 510006, P.R. China; [orcid.org/0000-0003-4502-7517](https://orcid.org/0000-0003-4502-7517)

**Shuai-Bing Zhang** – School of Chemistry and Environment Engineering, Changchun University of Science and Technology, Changchun 130022, P.R. China

**Run-Han Li** – Guangdong Provincial Key Laboratory of Carbon Dioxide Resource Utilization, School of Chemistry, South China Normal University, Guangzhou 510006, P.R. China

**Long-Zhang Dong** – Guangdong Provincial Key Laboratory of Carbon Dioxide Resource Utilization, School of Chemistry, South China Normal University, Guangzhou 510006, P.R. China

**Ming-Yi Yang** – Guangdong Provincial Key Laboratory of Carbon Dioxide Resource Utilization, School of Chemistry, South China Normal University, Guangzhou 510006, P.R. China

**Pei Huang** – Guangdong Provincial Key Laboratory of Carbon Dioxide Resource Utilization, School of Chemistry, South China Normal University, Guangzhou 510006, P.R. China

**Yu-Fei Liu** – Guangdong Provincial Key Laboratory of Carbon Dioxide Resource Utilization, School of Chemistry, South China Normal University, Guangzhou 510006, P.R. China

**Ze-Hui Li** – Guangdong Provincial Key Laboratory of Carbon Dioxide Resource Utilization, School of Chemistry, South China Normal University, Guangzhou 510006, P.R. China

**Han Zhang** – Guangdong Provincial Key Laboratory of Carbon Dioxide Resource Utilization, School of Chemistry, South China Normal University, Guangzhou 510006, P.R. China

**Shun-Li Li** – Guangdong Provincial Key Laboratory of Carbon Dioxide Resource Utilization, School of Chemistry, South China Normal University, Guangzhou 510006, P.R. China

Complete contact information is available at:  
<https://pubs.acs.org/10.1021/jacs.4c08951>

### Notes

The authors declare no competing financial interest.

## ACKNOWLEDGMENTS

We acknowledge the financial support from the National Key R&D Program of China (2023YFA1507204), the National Natural Science Foundation of China (22225109, 22071109, 22105080, and 22201083), the China National Postdoctoral Program for Innovative Talents (BX20220115), the Project funded by China Postdoctoral Science Foundation (2021M701270 and 2020M682748), the Guangdong Basic and Applied Basic Research Foundation (2023A1515010779 and 2023A1515010928), and the Guangzhou Basic and Applied Basic Research Fund Project (2024A04J2379).

## REFERENCES

- (1) Cote, A. P.; Benin, A. I.; Ockwig, N. W.; O’Keeffe, M.; Matzger, A. J.; Yaghi, O. M. Porous, crystalline, covalent organic frameworks. *Science* **2005**, *310* (5751), 1166–1170.
- (2) El-Kaderi, H. M.; Hunt, J. R.; Mendoza-Cortés, J. L.; Côté, A. P.; Taylor, R. E.; O’Keeffe, M.; Yaghi, O. M. Designed Synthesis of 3D Covalent Organic Frameworks. *Science* **2007**, *316* (5822), 268–272.
- (3) Uribe-Romo, F. J.; Hunt, J. R.; Furukawa, H.; Klock, C.; O’Keeffe, M.; Yaghi, O. M. A crystalline imine-linked 3-D porous covalent organic framework. *J. Am. Chem. Soc.* **2009**, *131* (13), 4570–4571.
- (4) Wan, S.; Guo, J.; Kim, J.; Ihée, H.; Jiang, D. A photoconductive covalent organic framework: self-condensed arene cubes composed of eclipsed 2D polypyrene sheets for photocurrent generation. *Angew. Chem., Int. Ed. Engl.* **2009**, *48* (30), 5439–42.
- (5) Ding, S. Y.; Gao, J.; Wang, Q.; Zhang, Y.; Song, W. G.; Su, C. Y.; Wang, W. Construction of Covalent Organic Framework for Catalysis: Pd/COF-LZU1 in Suzuki-Miyaura Coupling Reaction. *J. Am. Chem. Soc.* **2011**, *133* (49), 19816–19822.
- (6) Guan, Q.; Zhou, L.-L.; Dong, Y.-B. Metalated covalent organic frameworks: from synthetic strategies to diverse applications. *Chem. Soc. Rev.* **2022**, *51* (15), 6307–6416.
- (7) Sasmal, H. S.; Kumar Mahato, A.; Majumder, P.; Banerjee, R. Landscaping Covalent Organic Framework Nanomorphologies. *J. Am. Chem. Soc.* **2022**, *144* (26), 11482–11498.
- (8) Keller, N.; Bein, T. Optoelectronic processes in covalent organic frameworks. *Chem. Soc. Rev.* **2021**, *50* (3), 1813–1845.
- (9) Huang, N.; Wang, P.; Jiang, D. Covalent organic frameworks: a materials platform for structural and functional designs. *Nat. Rev. Mater.* **2016**, *1* (10), 16068.
- (10) Liang, R.-R.; Jiang, S.-Y.; A, R.-H.; Zhao, X. Two-dimensional covalent organic frameworks with hierarchical porosity. *Chem. Soc. Rev.* **2020**, *49* (12), 3920–3951.
- (11) Chen, X.; Geng, K.; Liu, R.; Tan, K. T.; Gong, Y.; Li, Z.; Tao, S.; Jiang, Q.; Jiang, D. Covalent Organic Frameworks: Chemical Approaches to Designer Structures and Built-In Functions. *Angew. Chem., Int. Ed.* **2020**, *59* (13), 5050–5091.
- (12) Pang, Z.-F.; Xu, S.-Q.; Zhou, T.-Y.; Liang, R.-R.; Zhan, T.-G.; Zhao, X. Construction of Covalent Organic Frameworks Bearing Three Different Kinds of Pores through the Heterostructural Mixed Linker Strategy. *J. Am. Chem. Soc.* **2016**, *138* (14), 4710–4713.
- (13) Yan, X.; Su, X.; Chen, J.; Jin, C.; Chen, L. Two-Dimensional Metal-Organic Frameworks towards Spintronics. *Angew. Chem., Int. Ed.* **2023**, *62*, No. e202305408.
- (14) Guan, X.; Fang, Q.; Yan, Y.; Qiu, S. Functional Regulation and Stability Engineering of Three-Dimensional Covalent Organic Frameworks. *Acc. Chem. Res.* **2022**, *55* (14), 1912–1927.
- (15) Gropp, C.; Ma, T.; Hanikel, N.; Yaghi, O. M. Design of higher valency in covalent organic frameworks. *Science* **2020**, *370* (6515), No. eabd6406.
- (16) Lin, G.; Ding, H.; Chen, R.; Peng, Z.; Wang, B.; Wang, C. 3D Porphyrin-Based Covalent Organic Frameworks. *J. Am. Chem. Soc.* **2017**, *139* (25), 8705–8709.
- (17) Ding, J.; Guan, X.; Lv, J.; Chen, X.; Zhang, Y.; Li, H.; Zhang, D.; Qiu, S.; Jiang, H.-L.; Fang, Q. Three-Dimensional Covalent

Organic Frameworks with Ultra-Large Pores for Highly Efficient Photocatalysis. *J. Am. Chem. Soc.* **2023**, *145* (5), 3248–3254.

- (18) Jin, F. Z.; Lin, E.; Wang, T. H.; Yan, D.; Yang, Y.; Chen, Y.; Cheng, P.; Zhang, Z. J. Rationally fabricating 3D porphyrinic covalent organic frameworks with scu topology as highly efficient photocatalysts. *Chem* **2022**, *8* (11), 3064–3080.
- (19) Gui, B.; Lin, G.; Ding, H.; Gao, C.; Mal, A.; Wang, C. Three-Dimensional Covalent Organic Frameworks: From Topology Design to Applications. *Acc. Chem. Res.* **2020**, *53* (10), 2225–2234.
- (20) Shan, Z.; Wu, M.; Zhu, D.; Wu, X.; Zhang, K.; Verduzco, R.; Zhang, G. 3D Covalent Organic Frameworks with Interpenetrated pcb Topology Based on 8-Connected Cubic Nodes. *J. Am. Chem. Soc.* **2022**, *144* (13), 5728–5733.
- (21) Liu, W.; Gong, L.; Liu, Z.; Jin, Y.; Pan, H.; Yang, X.; Yu, B.; Li, N.; Qi, D.; Wang, K.; Wang, H.; Jiang, J. Conjugated Three-Dimensional High-Connected Covalent Organic Frameworks for Lithium-Sulfur Batteries. *J. Am. Chem. Soc.* **2022**, *144* (37), 17209–17218.
- (22) Jin, F.; Lin, E.; Wang, T.; Geng, S.; Wang, T.; Liu, W.; Xiong, F.; Wang, Z.; Chen, Y.; Cheng, P.; Zhang, Z. Bottom-Up Synthesis of 8-Connected Three-Dimensional Covalent Organic Frameworks for Highly Efficient Ethylene/Ethane Separation. *J. Am. Chem. Soc.* **2022**, *144* (12), 5643–5652.
- (23) Jin, F.; Lin, E.; Wang, T.; Geng, S.; Hao, L.; Zhu, Q.; Wang, Z.; Chen, Y.; Cheng, P.; Zhang, Z. Rationally Fabricating Three-Dimensional Covalent Organic Frameworks for Propyne/Propylene Separation. *J. Am. Chem. Soc.* **2022**, *144* (50), 23081–23088.
- (24) Liang, L.; Qiu, Y.; Wang, W. D.; Han, J.; Luo, Y.; Yu, W.; Yin, G. L.; Wang, Z. P.; Zhang, L.; Ni, J.; Niu, J.; Sun, J.; Ma, T.; Wang, W. Non-Interpenetrated Single-Crystal Covalent Organic Frameworks. *Angew. Chem., Int. Ed.* **2020**, *59*, 17991.
- (25) Ma, T.; Kapustin, E. A.; Yin, S. X.; Liang, L.; Zhou, Z.; Niu, J.; Li, L.-H.; Wang, Y.; Su, J.; Li, J.; Wang, X.; Wang, W. D.; Wang, W.; Sun, J.; Yaghi, O. M. Single-crystal x-ray diffraction structures of covalent organic frameworks. *Science* **2018**, *361* (6397), 48–52.
- (26) Liu, R.; Tan, K. T.; Gong, Y.; Chen, Y.; Li, Z.; Xie, S.; He, T.; Lu, Z.; Yang, H.; Jiang, D. Covalent organic frameworks: an ideal platform for designing ordered materials and advanced applications. *Chem. Soc. Rev.* **2021**, *50* (1), 120–242.
- (27) Guan, X.; Chen, F.; Fang, Q.; Qiu, S. Design and applications of three dimensional covalent organic frameworks. *Chem. Soc. Rev.* **2020**, *49* (5), 1357–1384.
- (28) Kang, C.; Zhang, Z.; Kusaka, S.; Negita, K.; Usadi, A. K.; Calabro, D. C.; Baugh, L. S.; Wang, Y.; Zou, X.; Huang, Z.; Matsuda, R.; Zhao, D. Covalent organic framework atropisomers with multiple gas-triggered structural flexibilities. *Nat. Mater.* **2023**, *22* (5), 636–643.
- (29) Wei, L.; Sun, T.; Shi, Z.; Xu, Z.; Wen, W.; Jiang, S.; Zhao, Y.; Ma, Y.; Zhang, Y.-B. Guest-adaptive molecular sensing in a dynamic 3D covalent organic framework. *Nat. Commun.* **2022**, *13* (1), 7936.
- (30) Li, H.; Pan, Q.; Ma, Y.; Guan, X.; Xue, M.; Fang, Q.; Yan, Y.; Valtchev, V.; Qiu, S. Three-Dimensional Covalent Organic Frameworks with Dual Linkages for Bifunctional Cascade Catalysis. *J. Am. Chem. Soc.* **2016**, *138* (44), 14783–14788.
- (31) Zhao, Y.; Das, S.; Sekine, T.; Mabuchi, H.; Irie, T.; Sakai, J.; Wen, D.; Zhu, W.; Ben, T.; Negishi, Y. Record Ultralarge-Pores, Low Density Three-Dimensional Covalent Organic Framework for Controlled Drug Delivery. *Angew. Chem., Int. Ed.* **2023**, *62* (13), No. e202300172.
- (32) Yu, C.; Li, H.; Wang, Y.; Suo, J.; Guan, X.; Wang, R.; Valtchev, V.; Yan, Y.; Qiu, S.; Fang, Q. Three-Dimensional Triptycene-Functionalized Covalent Organic Frameworks with hea Net for Hydrogen Adsorption. *Angew. Chem., Int. Ed.* **2022**, *61* (13), No. e202117101.
- (33) Han, W. K.; Liu, Y.; Yan, X.; Jiang, Y.; Zhang, J.; Gu, Z. G. Integrating Light-Harvesting Ruthenium(II)-based Units into Three-Dimensional Metal Covalent Organic Frameworks for Photocatalytic Hydrogen Evolution. *Angew. Chem., Int. Ed.* **2022**, *61* (40), No. e202208791.
- (34) Gong, C.; Wang, H.; Sheng, G.; Wang, X.; Xu, X.; Wang, J.; Miao, X.; Liu, Y.; Zhang, Y.; Dai, F.; Chen, L.; Li, N.; Xu, G.; Jia, J.; Zhu, Y.; Peng, Y. Synthesis and Visualization of Entangled 3D Covalent Organic Frameworks with High-Valency Stereoscopic Molecular Nodes for Gas Separation. *Angew. Chem., Int. Ed.* **2022**, *61* (32), No. e202204899.
- (35) Lu, H.-S.; Han, W.-K.; Yan, X.; Chen, C.-J.; Niu, T.; Gu, Z.-G. A 3D Anionic Metal Covalent Organic Framework with soc Topology Built from an Octahedral TiIV Complex for Photocatalytic Reactions. *Angew. Chem., Int. Ed.* **2021**, *60* (33), 17881–17886.
- (36) Zhu, Q.; Wang, X.; Clowes, R.; Cui, P.; Chen, L.; Little, M. A.; Cooper, A. I. 3D Cage COFs: A Dynamic Three-Dimensional Covalent Organic Framework with High-Connectivity Organic Cage Nodes. *J. Am. Chem. Soc.* **2020**, *142* (39), 16842–16848.
- (37) Li, Z.; Xu, G.; Zhang, C.; Ma, S.; Jiang, Y.; Xiong, H.; Tian, G.; Wu, Y.; Wei, Y.; Chen, X.; Yang, Y.; Wei, F. Synthesis of 12-Connected Three-Dimensional Covalent Organic Framework with Inj Topology. *J. Am. Chem. Soc.* **2024**, *146* (7), 4327–4332.
- (38) Lin, G.; Ding, H.; Yuan, D.; Wang, B.; Wang, C. A Pyrene-Based, Fluorescent Three-Dimensional Covalent Organic Framework. *J. Am. Chem. Soc.* **2016**, *138* (10), 3302–3305.
- (39) Lin, S.; Diercks, C. S.; Zhang, Y. B.; Kornienko, N.; Nichols, E. M.; Zhao, Y.; Paris, A. R.; Kim, D.; Yang, P.; Yaghi, O. M.; Chang, C. J. Covalent organic frameworks comprising cobalt porphyrins for catalytic CO<sub>2</sub> reduction in water. *Science* **2015**, *349* (6253), 1208–1213.
- (40) Nguyen, H. L.; Gandara, F.; Furukawa, H.; Doan, T. L.; Cordova, K. E.; Yaghi, O. M. A Titanium-Organic Framework as an Exemplar of Combining the Chemistry of Metal- and Covalent-Organic Frameworks. *J. Am. Chem. Soc.* **2016**, *138* (13), 4330–4333.
- (41) Luo, J.; Zhang, J. Donor-Acceptor Fluorophores for Visible-Light-Promoted Organic Synthesis: Photoredox/Ni Dual Catalytic C(sp<sup>3</sup>)-C(sp<sup>2</sup>) Cross-Coupling. *ACS Catal.* **2016**, *6* (2), 873–877.
- (42) Ishimatsu, R.; Matsunami, S.; Kasahara, T.; Mizuno, J.; Edura, T.; Adachi, C.; Nakano, K.; Imato, T. Electrogenated Chemiluminescence of Donor-Acceptor Molecules with Thermally Activated Delayed Fluorescence. *Angew. Chem., Int. Ed.* **2014**, *53* (27), 6993–6996.
- (43) Uoyama, H.; Goushi, K.; Shizu, K.; Nomura, H.; Adachi, C. Highly efficient organic light-emitting diodes from delayed fluorescence. *Nature* **2012**, *492* (7428), 234–238.
- (44) Jati, A.; Dey, K.; Nurhuda, M.; Addicoat, M. A.; Banerjee, R.; Maji, B. Dual Metalation in a Two-Dimensional Covalent Organic Framework for Photocatalytic C-N Cross-Coupling Reactions. *J. Am. Chem. Soc.* **2022**, *144* (17), 7822–7833.
- (45) Na, H.; Mirica, L. M. Deciphering the mechanism of the Ni-photocatalyzed C-O cross-coupling reaction using a tridentate pyridinophane ligand. *Nat. Commun.* **2022**, *13* (1), 1313.
- (46) Yuan, M.; Song, Z.; Badir, S. O.; Molander, G. A.; Gutierrez, O. On the Nature of C(sp<sup>3</sup>)-C(sp<sup>2</sup>) Bond Formation in Nickel-Catalyzed Tertiary Radical Cross-Couplings: A Case Study of Ni/Photoredox Catalytic Cross-Coupling of Alkyl Radicals and Aryl Halides. *J. Am. Chem. Soc.* **2020**, *142* (15), 7225–7234.
- (47) Li, J.; Huang, C.-Y.; Li, C.-J. Two-in-one metallaphotoredox cross-couplings enabled by a photoactive ligand. *Chem* **2022**, *8* (9), 2419–2431.
- (48) Wang, X.; Ding, X.; Jin, Y.; Qi, D.; Wang, H.; Han, Y.; Wang, T.; Jiang, J. Post-Nickelation of a Crystalline Trinuclear Copper Organic Framework for Synergistic Photocatalytic Carbon Dioxide Conversion. *Angew. Chem., Int. Ed.* **2023**, *62* (18), No. e202302808.
- (49) Chen, Y.; Liu, A.-G.; Liu, P.-D.; Chen, Z.-T.; Liu, S.-Y.; Li, B. Enhancing energy transfer through visible-light-driven polymerization in a metal-organic framework. *J. Mater. Chem. A* **2023**, *11* (34), 18236–18246.
- (50) Cavedon, C.; Gisbertz, S.; Reischauer, S.; Vogl, S.; Sperlich, E.; Burke, J. H.; Wallick, R. F.; Schrottke, S.; Hsu, W.-H.; Anghileri, L.; Pfeifer, Y.; Richter, N.; Teutloff, C.; Müller-Werkmeister, H.; Cambié, D.; Seeberger, P. H.; Vura-Weis, J.; van der Veen, R. M.; Thomas, A.; Pieber, B. Intraligand Charge Transfer Enables Visible-Light-



Mediated Nickel-Catalyzed Cross-Coupling Reactions\*\*. *Angew. Chem., Int. Ed.* **2022**, *61* (46), No. e202211433.

(51) Gilmanova, L.; Bon, V.; Shupletsov, L.; Pohl, D.; Rauche, M.; Brunner, E.; Kaskel, S. Chemically Stable Carbazole-Based Imine Covalent Organic Frameworks with Acidochromic Response for Humidity Control Applications. *J. Am. Chem. Soc.* **2021**, *143* (44), 18368–18373.

(52) Fan, Y.; Kang, D. W.; Labalme, S.; Li, J.; Lin, W. Enhanced Energy Transfer in A  $\pi$ -Conjugated Covalent Organic Framework Facilitates Excited-State Nickel Catalysis. *Angew. Chem., Int. Ed.* **2023**, *62* (11), No. e202218908.

(53) Lan, G.; Quan, Y.; Wang, M.; Nash, G. T.; You, E.; Song, Y.; Veroneau, S. S.; Jiang, X.; Lin, W. Metal-Organic Layers as Multifunctional Two-Dimensional Nanomaterials for Enhanced Photoredox Catalysis. *J. Am. Chem. Soc.* **2019**, *141* (40), 15767–15772.

(54) Madrahimov, S. T.; Gallagher, J. R.; Zhang, G.; Meinhart, Z.; Garibay, S. J.; Delferro, M.; Miller, J. T.; Farha, O. K.; Hupp, J. T.; Nguyen, S. T. Gas-Phase Dimerization of Ethylene under Mild Conditions Catalyzed by MOF Materials Containing (bpy)NiII Complexes. *ACS Catal.* **2015**, *5* (11), 6713–6718.

(55) Li, S.; Wang, B.; Liu, G.; Li, X.; Sun, C.; Zhang, Z.; Wang, X. Achieving ultra-trace analysis and multi-light driven photodegradation toward phenolic derivatives via a bifunctional catalyst derived from a Cu(i)-complex-modified polyoxometalate. *Inorg. Chem. Front.* **2024**, *11* (5), 1561–1572.

(56) Li, S.; Sun, J.; Liu, G.; Zhang, S.; Zhang, Z.; Wang, X. A new Keggin-type polyoxometallate-based bifunctional catalyst for trace detection and pH-universal photodegradation of phenol. *Chin. Chem. Lett.* **2024**, *35* (8), 109148.

(57) Yang, H. B.; Hung, S.-F.; Liu, S.; Yuan, K.; Miao, S.; Zhang, L.; Huang, X.; Wang, H.-Y.; Cai, W.; Chen, R.; Gao, J.; Yang, X.; Chen, W.; Huang, Y.; Chen, H. M.; Li, C. M.; Zhang, T.; Liu, B. Atomically dispersed Ni(i) as the active site for electrochemical CO<sub>2</sub> reduction. *Nature Energy* **2018**, *3* (2), 140–147.